Influence of Ionic Strength, Actin State, and Caldesmon Construct Size on the Number of Actin Monomers in a Caldesmon Binding Site†

Scott Fredricksen, Anmei Cai, Boris Gafurov, Andrea Resetar, and Joseph M. Chalovich*

Department of Biochemistry and Molecular Biology, The Brody School of Medicine at East Carolina University, 600 Moye Boulevard, Greenville, North Carolina 27858-4354

Received December 20, 2002; Revised Manuscript Received March 28, 2003

ABSTRACT: There is no consensus on the mechanism of inhibition of actin−myosin ATPase activity by caldesmon. Various models are based on different assumptions for the number of actin monomers that constitute a caldesmon binding site. Differences in binding behavior may be due to variations in the assay, the range of caldesmon concentrations, the type of caldesmon, and the method of data analysis used. We have evaluated these factors by measuring binding in the presence and absence of tropomyosin with both intact caldesmon and a recombinant 35 kDa actin binding fragment and with actin initially in the polymerized state or monomeric state. In all cases caldesmon binding could be simulated with a model having one class of binding sites. However, the number of actin monomers constituting a site was variable. Binding to F-actin at 165 mM ionic strength was best described with 7 actin monomers per site. When caldesmon bound to actin during the polymerization of G-actin, the size of the binding site was 3. Binding of the expressed truncated fragment, Cad35, could be described with 3 monomers per site. A simple interpretation of the data is that caldesmon binds tightly to 2−3 actin monomers. Additional parts of caldesmon bind less tightly to actin, causing caldesmon to cover approximately 7 actin monomers. The appendix contains an analysis of several binding curves with multiple binding site models. There is no compelling evidence for two classes of binding sites.

Caldesmon is an actin binding protein that is found in smooth muscle and nonmuscle cells. Since its discovery (*1*), caldesmon has generated considerable interest in the field of smooth muscle contraction because of the possibility that caldesmon acts as a secondary control of smooth muscle contraction (*2*).

Caldesmon binding to actin results in inhibition of the actin-activated ATPase activity of myosin (*3*−*6*) and its subfragments (*7*, *8*). This inhibition is enhanced by the presence of tropomyosin (*6*), but the requirement for tropomyosin is controversial (*8*). Tropomyosin changes the relationship between ATPase activity and the fraction of actin containing bound caldesmon. In the absence of tropomyosin there is a linear decrease in ATPase activity with bound caldesmon concentration (*9*, *10*). In the presence of tropomyosin, the ATPase activity at zero caldesmon is higher, and the rate declines more rapidly in a curvilinear fashion as the caldesmon concentration is increased (*9*, *10*). Caldesmon alters the position of tropomyosin on actin (*11*) but in a manner that is different from the effect of troponin in striated muscle. Caldesmon is a competitive inhibitor of myosin binding (*8*, *10*, *12*−*16*) in both the presence and absence of tropomyosin. Caldesmon could have a dual effect on ATPase activity by reversing both the potentiation of ATPase activity and the binding of S1[1]−ATP to actin. The relative importance of these two effects is unsettled. There is no consensus on the mechanism of regulation by caldesmon. The differences in models are based on different interpretations of some basic properties of caldesmon (*17*) including its mode of binding to actin.

In one model, caldesmon acts much like troponin, the heterotrimeric protein that regulates contraction in striated muscle. A single caldesmon molecule is thought to bind to 1 actin monomer, and inhibition of actin-activated ATPase activity requires virtually 1 caldesmon bound per actin monomer (90% inhibition requires 0.7 caldesmon bound per actin) (*18*). Tropomyosin changes the binding so that caldesmon binds tightly to sites composed of about 14 actin monomers and weakly to single actin protomers. The original data were interpreted as high-affinity binding to about 22−34 actin protomers and weak binding to about 4 actin monomers (*9*, *19*). An expressed fragment from the COOH region of caldesmon, 685C, bound to actin in a similar way as full-length caldesmon and likewise inhibited ATPase activity in the same manner (*19*). The biphasic binding curve was used to support the idea of interaction with 14 actin monomers. Another fragment produced by CNBr digestion

† This work was supported by Grant AR35216 from the National Institutes of Health and a fellowship from the North Carolina Affiliate of the American Heart Association to S.F. Preliminary reports of these data have been presented at the Second Seidel Symposium, April 11−14, 1999, Woods Hole, MA, and the Biophysical Society Meeting, March 1−5, 2003, San Antonio, TX.

* To whom correspondence should be addressed. Telephone: (252) 744-2973. Fax: (252) 744-3383. E-mail: chalovichj@mail.ecu.edu.

[1] Abbreviations: EDTA, ethylenediaminetetraacetic acid; EGTA, ethylene glycol bis(β-aminoethyl ether)-*N*,*N*,*N*′,*N*′-tetraacetic acid; IANBD, *N*-[2-(iodoacetoxy)ethyl]-*N*-methylamino-7-nitrobenz-2-oxa-1,3-diazole; S1, myosin subfragment 1.

10.1021/bi0274017 CCC: $25.00
Published on Web 05/03/2003

and having a molecular mass of about 10 kDa was reported to bind with a stoichiometry of one 10 kDa fragment per 7 actin monomers (*20*) even though this fragment is too small to physically contact 7 actin monomers. However, a similar fragment was found to bind to actin in a 1:1 complex by another laboratory (*21*). The ability of a single caldesmon molecule, or a part of a caldesmon molecule, to bind strongly to a large number of actin monomers ($\geq$14) and inhibit the ATPase activity of a similar number of actin monomers was attributed to the stabilization of an inhibitory position of tropomyosin on actin (*19*).

In another model, caldesmon inhibits ATPase activity largely because of displacement of the ATP complex of myosin subfragments from actin and actin−tropomyosin. Caldesmon binds to $\approx$7 actin monomers (*7*, *22*−*27*) in both the presence and absence of tropomyosin. Caldesmon binding to actin−tropomyosin excludes S1−ATP from most, if not all, of those actin monomers within a single binding site (*8*, *14*, *15*). In this respect caldesmon differs from troponin (*17*). Fragments of caldesmon produced by enzymatic digestion bind to a variable number of actin monomers in actin−tropomyosin in proportion to the size of the fragment. A chymotryptic 35 kDa COOH-terminal fragment bound to 3−4 actin monomers (*28*). A chymotryptic 20 kDa COOH-terminal fragment of caldesmon bound to 2 actin monomers (*29*) while a 7.3 kDa fragment binds with a 1:1 stoichiometry (*30*). Inhibition of ATPase activity occurs roughly in parallel with a decrease in binding of S1−ATP to actin as the concentration of a 20 kDa fragment is increased (*29*). These data suggest that caldesmon is a side binding protein that covers most of the binding sites for the low-affinity interaction between myosin−ATP and actin. Electron microscopic images of caldesmon−actin support this view (*31*).

To resolve these two models, we sought evidence for two types of caldesmon−actin interaction: a 1:1 association of caldesmon with an actin protomer and an interaction of 1 caldesmon with 14 or more actin protomers. We were unsuccessful. Rather, we found that the caldesmon site normally consists of 5−7 actin protomers depending on the conditions. We tried to maximize the number of caldesmon molecules bound to actin by adding intact caldesmon to polymerizing actin. Under these conditions we were able to obtain 1 caldesmon bound per 3 actin monomers. A bacterially expressed 35 kDa COOH-terminal fragment of caldesmon bound to a single population of sites in F-actin consisting of 3 actin monomers. Tropomyosin does not appear to affect the size of the binding site with either intact caldesmon or with Cad35. We suggest that caldesmon interacts strongly with 2−3 actin monomers and less tightly with an additional 3−4 monomers. When high concentrations of caldesmon are added to a growing actin chain, the favored interaction consists of 2−3 actin monomers. This does not seem to represent the normal cellular state.

Alternative models of caldesmon binding to actin are described in the appendix. Neither the results described here nor the results from other laboratories require that in the presence of tropomyosin there are two modes of binding of caldesmon to actin. Rather, caldesmon binding to actin seems to occur by essentially the same mechanism in both the presence and absence of tropomyosin. Binding to polymerized actin occurs as a single population in which 1 caldesmon interacts with 5−7 actin protomers.

EXPERIMENTAL PROCEDURES

Preparation of Cad35. The actin binding region of caldesmon, reaching from Met 461 to Pro 771, Cad35, was subcloned in the pSBET-A expression vector (*32*) and afterward expressed in *Escherichia coli*. We received the full-length chicken gizzard caldesmon cDNA from Dr. Joseph Bryan and used it as a template in a polymerase chain reaction (PCR) to produce the cDNA fragment coding for the 35 kDa actin binding region. Suitable restriction sites at either end of the cDNA were introduced by PCR, namely, *Nde*I at the 5′ end and *Bam*HI at the 3′ end. The primers used in the PCR were the 5′ primer 5′-AGAGAGCATAT-GAAAGAGTGTC-3′ and the 3′ primer 5′-CCCGGATCCT-TATTACGGTTCTTTCTCAAA-3′. The *Nde*I/*Bam*HI restriction enzyme-digested PCR product was purified and inserted at the same restriction sites of the pSBETA expression vector (from Dr. H.-H. Steinbiss). This vector permits overexpression of the AGA/AGG-rich caldesmon sequence in *E. coli* without mistranslation of AGA codons into Lys instead of Arg (*33*). The DNA sequence was confirmed using the cyclist EXO-pfu DNA sequencing kit (Stratagene) and additionally by cycle sequencing with the ABI prism big dye terminator cycle sequencing ready reaction kit and resolving the products on an ABI prism 377 automated sequencer (Perkin-Elmer/Applied Biosystems).

Protein Expression and Purification. Cad35 was expressed in freshly transformed *E. coli* NovaBlue (DE3) bacteria (Novagen). Six liters of LB medium containing 0.035 mg/mL kanamycin was inoculated with a 3 mL preculture. The bacteria were grown for 16−20 h at 37 °C on an orbital shaker; induction with isopropyl β-D-thiogalactopyranoside was not required. The bacteria were harvested by centrifugation at 5000*g* for 15 min at 4 °C. Expression of Cad35 was checked by electrophoresis.

Cad35 was purified at 4 °C from the bacterial pellet. The pellet was suspended in 5 mL of buffer/g of pellet (25% sucrose, 50 mM Tris-HCl, pH 8.0, 2 mM EGTA, 2 mM EDTA, 2 mM DTT, 0.01% NaN_3), and protease inhibitor cocktail (Sigma-Aldrich P8465; 0.25 mL/g of bacteria pellet) was added. Bacteria were lysed either using four cycles of freeze/thaw or by addition of a freshly made lysozyme solution (40 μL of 20 mg/mL per gram of pellet) and subsequent incubation for 45−60 min. After the sodium chloride concentration was increased to 0.6 M final, the sample was sonicated with a sonicator cell disruptor (6 $\times$ 30 s bursts at 25% duty cycle). The sample was then centrifuged at 36000*g* for 25 min, and the supernatant was dialyzed twice against 2 L of Q-Sepharose buffer (10 mM imidazole, pH 7.5, 200 mM NaCl, 2 mM DTT, 0.01% NaN_3, protease inhibitor cocktail (Sigma-Aldrich P8465; 1 mL/4 g of bacteria pellet). The sample was clarified by centrifugation and loaded on a 25 mL Q-Sepharose (Amersham-Pharmacia) column, equilibrated with the same buffer. Cad35 did not bind to this resin. The Cad35 was dialyzed twice against 2 L of Affi-Cam buffer (25 mM Tris-HCl, pH 7.5, 1 mM $CaCl_2$, 100 mM NaCl, 1 mM $MgCl_2$, 2 mM DTT, 0.01% NaN_3) and loaded onto an equilibrated calmodulin affinity column. Recombinant calmodulin was prepared from the pT7-7-Cam clone (from Dr. Madeline Shea) according to ref *34* and coupled to Affi-Gel 10 (Bio-Rad) according to the manufacturer's directions. Pure Cad35 was eluted with

30 mM Tris−MES, pH 7.0, 100 mM NaCl, 1 mM EGTA, 1 mM EDTA, 2 mM DTT, and 0.01% NaN_3. The typical yield of Cad35 was approximately 10 mg/L of initial culture.

The molecular mass of the protein product was verified at the Mass Spectrometry Facility of the North Carolina State University Department of Chemistry. The Cad35 fragment was dialyzed into 1 M acetic acid and analyzed by ion-spray mass spectroscopy. The mass spectrum showed a single peak corresponding to a molecular mass of 34629, consistent with the theoretical molecular mass calculated from the amino acid sequence encoded by the pSBET-A Cad35 plasmid, 34631. A small second peak, consistent with a molecular mass of an additional 38 or 39 mass units, was also present and is consistent with the presence of a potassium ion as an adduct. Of note was the absence of peaks that differed by multiples of 28, the molecular mass difference between arginine and lysine. This result indicates a high level of homogeneity for our Cad35 protein preparations that contain no detectable levels of protein containing Arg-to-Lys substitutions.

Muscle Protein Preparations. Skeletal actin (*35*, *36*) and myosin (*37*) were isolated from rabbit back and leg muscle. Myosin S1 was made by digestion with chymotrypsin (*38*). Tropomyosin was isolated from turkey gizzards either by the method of Bretscher (*39*) or by the method of Graceffa et al. (*40*). The latter method does not use heat treatment. Turkey gizzard caldesmon was purified either by a method that involves heat treatment (*10*, *39*) or by a method that avoids heat treatment (*10*). In some cases caldesmon was labeled with [^{14}C]iodoacetamide (*10*) or IANBD (*41*).

Protein concentrations were determined spectrophotometrically using the following extinction coefficients ($\epsilon^{0.1\%}$) for 280 nm: actin, 1.15; myosin−S1, 0.75; Cad35, 0.7 mL mg^{-1} cm^{-1}. The extinction coefficient ($\epsilon^{0.1\%}$) for Cad35 was measured to be 0.7 using a published procedure (*42*). The absorbance at 280 nm was corrected for scattering by subtracting the absorbance at 340 nm. The Lowry assay (*43*) was employed for measuring concentrations of smooth muscle tropomyosin using bovine serum albumin as a standard.

Actin Binding Experiments. Actin was diluted to a concentration of 40 μM in binding buffer containing 34 mM potassium propionate, 10 mM imidazole, pH 7.0, 2 mM $MgCl_2$, 1 mM EGTA, 1 mM dithiothreitol, and 40 μM phalloidin and allowed to incubate overnight to lower the critical concentration of actin. Mixtures of phalloidin−actin, tropomyosin, and caldesmon in an appropriate buffer (binding buffer plus potassium propionate) in a 1 mL volume were centrifuged at 25 °C for 30 min at 45000 rpm in a Beckman TI50 rotor. Each pellet was incubated for 1−2 h in SDS sample buffer and then homogenized in a bath sonicator. Ten microliters of each sample was electrophoresed on 10% polyacrylamide gels. Scanned images of the gels were analyzed using Image Quant v.3.3 software (Molecular Dynamics). Densities obtained were converted into actual molar concentrations using calibration curves constructed from standard proteins. Standards were included on each gel.

Binding measurements in the presence of tropomyosin required special attention because tropomyosin migrates as two bands on electrophoresis. One of the bands comigrated with actin while the second band had a higher mobility than actin. The two tropomyosin bands were of the same intensity, so the area of the actin band was determined by subtracting the area of the lower tropomyosin band from the area corresponding to actin and the upper tropomyosin band.

Measurement of the composition of actin pellets was also done with reverse-phase HPLC. In that case, the protein pellets formed after sedimentation were mixed with 50 μL of 0.1% TFA in H_2O. After a 1−2 h incubation, the samples were sonicated. Fifty microliters of each sample was chromatographed on a μBondapak C18 column (Waters Inc.) equilibrated with 20% acetonitrile and 0.1% TFA. The column was washed with the same buffer at 1 mL/min, and the proteins were eluted with a gradient to 70% acetonitrile over 25 min. The retention times for caldesmon, tropomyosin, and actin were 12, 18, and 22 min, respectively. The protein peaks were monitored at 214 nm and analyzed using Chrom Perfect Spirit Tiger II (Justice Laboratory) software. Standard curves were used to calculate the protein concentrations.

Binding studies were also performed by mixing caldesmon and tropomyosin with G-actin and allowing the actin to polymerize. In such situations, the actin was initially in G-actin buffer (2 mM Tris-HCl, pH 8.0, 2 mM ATP, 0.2 mM $CaCl_2$, 0.005% NaN_3, 0.5 mM β-mercaptoethanol). Additions were made in the following order: tropomyosin, caldesmon, and binding buffer containing phalloidin. Samples were well stirred and incubated for at least 24 h at 0 °C prior to sedimentation.

In all cases, the ratio of bound actin to total actin (theta) and the free caldesmon concentration were calculated from the protein concentrations. The free caldesmon concentration was calculated from the difference between the total and bound concentrations. Because caldesmon occupies several actin protomers in an actin filament, there is a parking problem with caldesmon binding. Binding of a long ligand to a lattice of sites can be analyzed with the McGhee and von Hippel equation (*44*):

$$\frac{\nu}{L} = K(1 - n\omega)\left(\frac{(2\omega - 1)(1 - n\nu) + \nu - R}{2(\omega - 1)(1 - n\nu)}\right)^{n-1} \times \left(\frac{1 - (n + 1)\nu + R}{2(1 - n\nu)}\right)^{2} \quad (1)$$

where

$$R = \sqrt{(1 - (n + 1)\nu)^2 + 4\omega\nu(1 - n\nu)}$$

The parameters defining the binding are the number of actin monomers making a single binding site (n), the affinity of caldesmon to an isolated site of n protomers (K), and the cooperativity parameter (ω). Values of $\omega > 1$ indicate a favorable end-to-end interaction among adjacent caldesmon molecules. An expanded version of this equation and more detailed analyses of binding data are given in the appendix.

ATPase Activity Measurements. The rate of release of [^{32}P]-P_i from [γ-^{32}P]ATP was measured as described earlier (*45*).

Gel Electrophoresis. Proteins were analyzed by polyacrylamide gel electrophoresis by the method of Laemmli (1970) using a Mini-Protein II system (Bio-Rad Laboratories). Acrylamide stock solutions containing 29.2% acrylamide and 0.8% *N*,*N*′-methylenebis(acrylamide) were from National Diagnostics. Gels were stained with 0.1% Coomassie Brilliant Blue R350.

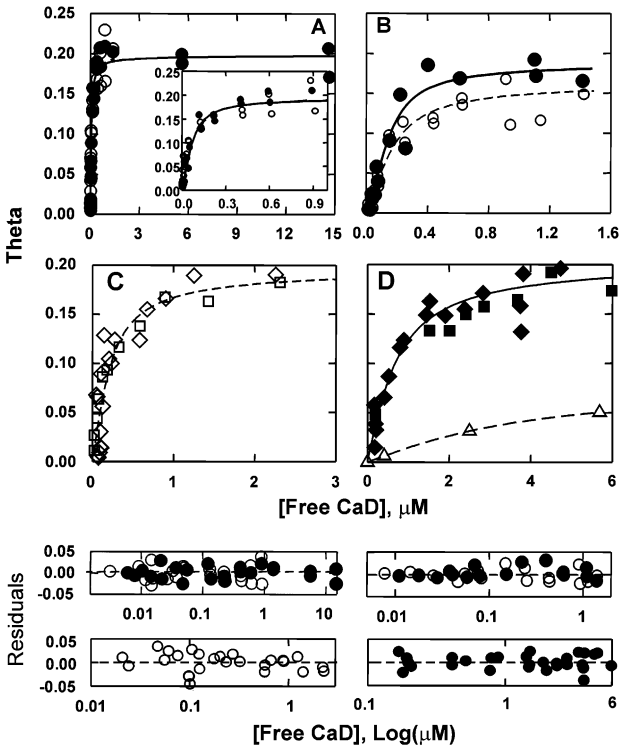

FIGURE 1: Binding of whole caldesmon to F-actin (open symbols) and F-actin−tropomyosin (closed symbols) with the electrophoresis method. Theta is the fraction of actin that has bound caldesmon. Insets show an expanded view of the data. Residuals shown at the bottom of the figure follow the same pattern as the parent curves. Residuals are shown as the difference between the measured and theoretical values against the Log of the free caldesmon concentration. All binding studies were done at 25 °C in binding buffer (34 mM potassium propionate, 10 mM imidazole, pH 7, 2 mM $MgCl_2$, 1 mM EGTA) with additional potassium propionate added to reach the desired ionic strength. (A) Non-heat-treated and unlabeled caldesmon in the following conditions binding to 0.5 μM actin ± 0.1 μM tropomyosin at 48 mM ionic strength. In the absence of tropomyosin $n = 5.5$, $\omega = 8.2$, and $K = 2.2$ μM^{-1}. In the presence of tropomyosin $n = 5.0$, $\omega = 9.5$, and $K = 1.2$ μM^{-1}. (B) NBD-labeled caldesmon binding to 0.5 μM actin ± 0.1 μM tropomyosin at 48 mM ionic strength. In the absence of tropomyosin $n = 6.0$, $\omega = 12.2$, and $K = 0.4$ μM^{-1}. In the presence of tropomyosin $n = 5.2$, $\omega = 14.2$, and $K = 0.4$ μM^{-1}. (C) Binding of heat-treated ^{14}C-labeled caldesmon to 7 μM actin at 60 mM ionic strength: $n = 5.0$, $\omega = 6.7$, and $K = 0.5$ μM^{-1}. (D) Binding of ^{14}C-labeled caldesmon to 7 μM actin at both 160 (diamonds and squares) and 600 mM ionic strength (triangles). At 160 mM ionic strength $n = 4.8$, $\omega = 4.8$, and $K = 0.2$ μM^{-1}. The curve shown for the 600 mM ionic strength condition is for $n = 11.9$, $\omega = 12.3$, and $K = 0.015$ μM^{-1}. In (C) and (D) the amount of caldesmon in the actin pellet was measured both by electrophoresis (diamonds) and by scintillation counting (squares and triangles).

Plasmid DNA and PCR reaction samples were analyzed by agarose gel electrophoresis on gels containing 1% molecular biology grade agarose (FMC BioProducts) using a flatbed apparatus (Owl Scientific). Ladders from Gibco BRL were used as size standards for all electrophoresis runs.

RESULTS

We explored several factors that may contribute to differences in binding of caldesmon to actin observed by various laboratories. Figure 1 shows a survey of binding studies done with intact caldesmon. The fraction of actin with bound caldesmon or theta is shown as a function of the free caldesmon concentration. Figure 1A shows the binding of non-heat-treated caldesmon to actin and to actin−tropomyosin. This binding curve was obtained at 48 mM ionic strength to enhance the binding so that an end point could be reached. There was no appreciable change in the amount of bound caldesmon between 1.5 and 15 μM free caldesmon. The number of actin monomers in a binding site or n is given by $1/\text{theta}_{max}$. That value was about 5. The inset to Figure 1A shows an expanded view of the binding curve at low free caldesmon concentrations. The shape of the curve does not suggest multiple populations of binding sites. The binding curves shown are best fits of the McGhee and von Hippel equation for a single class of sites. The theoretical curves describe the data well over the full range of concentrations examined. This can be clearly seen by an examination of the residuals (difference between experimental and theoretical values) shown at the bottom of the figure. The residuals are plotted against the log of the free caldesmon concentration to allow examination of the whole concentration range. The concentration range was varied by more than a factor of 10^3.

Figure 1B shows the binding of NBD-labeled caldesmon to actin−tropomyosin at 48 mM ionic strength measured with the gel electrophoresis method. The binding curve saturated at approximately 1 caldesmon per 5−6 actin monomers. An examination of the residuals shows that the theoretical curve for a single class of binding sites describes the data well over the whole concentration range.

Panels C and D of Figure 1 show binding curves at 60, 160, and 600 mM ionic strength. The direct plots and the residual plots show good agreement between the theoretical curves and the data. There is no evidence for multiple binding sites. Panels C and D of Figure 1 are of special interest because the caldesmon used was labeled with [^{14}C]iodoacetamide and binding was measured both by the electrophoresis method (diamonds) and by scintillation counting (squares and triangles) as in our earlier work. The binding curves obtained with the two methods are very similar.

If caldesmon is able to bind to actin in multiple ways, then it might be possible to bias one type of interaction by varying the conditions of binding. Figure 1 showed that changes in ionic strength and chemical modification of caldesmon had little effect on the binding. Another potential means of altering the distribution of caldesmon on actin was to add caldesmon to actin during actin polymerization. Binding of caldesmon to actin is much faster than actin polymerization so close packing of caldesmon on actin would be favored. Figure 2 shows that the binding curves measured during actin polymerization were very different from those measured with actin filaments. Varying concentrations of caldesmon were mixed with G-actin, and polymerization was initiated by the addition of a buffer containing $MgCl_2$. Figure 2A gives the results of experiments done at 0.5 μM G-actin. The amount of caldesmon bound was measured by gel electrophoresis. Theoretical curves are shown for several cases differing in actin concentration or method of measurement. The best fit for the data of Figure 2A occurred with $n = 2.5$ ($R^2 = 0.81$). The residuals for that fit are randomly distributed. Theoretical curves for $n = 2$ (upper dashed curve; $R^2 = 0.78$) and $n = 3$ (lower dashed curve; $R^2 = 0.79$) do not fit the data as well even though the values of K and ω were optimized.

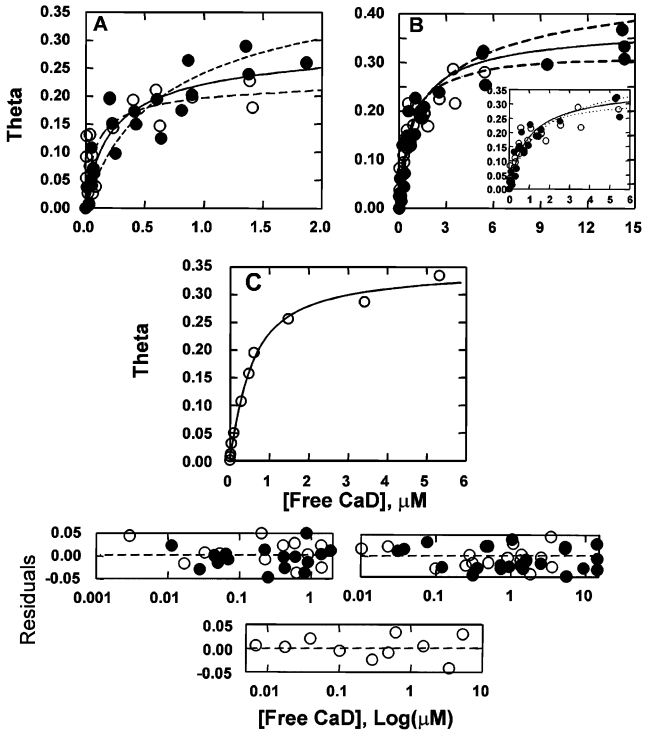

FIGURE 2: Binding of whole caldesmon to actin during polymerization. To a 100 μM G-actin stock in 2 mM Tris-HCl, 2 mM ATP, 0.2 mM $CaCl_2$, 0.005% NaN_3, and 0.5 mM β-mercaptoethanol, pH 8.0, was added tropomyosin (when appropriate) and caldesmon in a buffer to bring the final conditions to approximately 34 mM KCl, 2 mM $MgCl_2$, 1 mM EGTA, 1 mM dithiothreitol, and 10 mM imidazole, pH 7.0. Solid symbols indicate the presence of tropomyosin. Solid curves are best fits of the models, and dashed lines show alternate fits. Residuals shown at the bottom of the figure follow the same pattern as the parent curves. (A) The total G-actin was 0.5 μM, and the binding was determined by gel densitometry. $n = 2.5$, $\omega = 1.1$, and $K = 0.7$ μM^{-1} with 0.1 μM tropomyosin (upper and lower dashed lines show $n = 2$ and 3, respectively); $n = 3.3$, $\omega = 1.1$, and $K = 1.2$ μM^{-1} without tropomyosin (curve not shown). (B) The total G-actin was 2 μM, and the binding was determined by gel densitometry. $n = 3.0$, $\omega = 1.1$, and $K = 0.7$ μM^{-1} with 0.4 μM tropomyosin (upper and lower dashed lines show $n = 2.5$ and 3.5, respectively); $n = 3.1$, $\omega = 1.7$, and $K = 0.5$ μM^{-1} without tropomyosin (curve not shown). (C) The total G-actin was 2 μM without tropomyosin, and the binding was determined by HPLC. $n = 2.8$, $\omega = 3.2$, and $K = 0.5$ μM^{-1}.

In an attempt to better define the value of *n*, additional data were collected at higher actin concentrations. The data in Figure 2B were determined by the gel electrophoresis method while those in Figure 2C were obtained by reverse-phase HPLC. Both measurements gave similar results with $n = 3$. Figure 2B shows that the values of *n*, ω, and *K* describing the binding are similar in the presence and absence of tropomyosin. The data are well described with a single theoretical curve over the entire range of concentrations ($R^2 = 0.91$). The fit to the low concentration data can be more readily seen by the inset to Figure 2B and by the residuals. Upper and lower dashed lines show theoretical curves for $n = 2.5$ ($R^2 = 0.84$) and 3.5 ($R^2 = 0.83$), respectively. The most likely number of actin protomers interacting with caldesmon under these conditions is 3.

The greatest variation in reported binding values comes with studies of caldesmon fragments. Studies done with fragments produced by enzymatic digestion of intact caldesmon tend to show that small caldesmon fragments interact with fewer actin protomers than does intact caldesmon. In contrast, bacterially expressed caldesmon fragments have been reported to interact with 14 or more actin protomers in the presence of tropomyosin (*19*). To determine if these differences resulted from the method of preparing fragments, we prepared a recombinant COOH-terminal fragment of caldesmon for use in binding studies. That 35 kDa fragment was chosen because it contains all of the key sites thought to be important for binding to both tropomyosin and actin (*46*). Also, a similar fragment, produced by enzymatic digestion, was nearly as effective as intact caldesmon in inhibiting the attachment of myosin to actin in muscle fiber preparations (*47*).

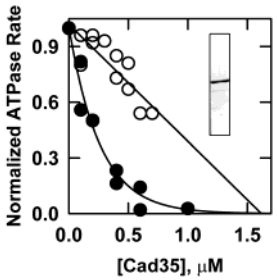

FIGURE 3: Effect of tropomyosin on the inhibition of actin-activated ATPase activity by Cad35. ATPase rates were normalized to allow comparison of data in the absence (open symbols) and presence (closed symbols) of tropomyosin. Conditions: 5 μM actin ± 1.1 μM tropomyosin, 1 μM S1, 36 mM potassium propionate, 2 mM $MgCl_2$, 1 mM MgATP, 5 mM dithiothreitol, and 10 mM imidazole, pH 7, at 25 °C. The inset shows an SDS gel of the expressed Cad35.

The expressed Cad35 was an effective inhibitor of actin-activated ATPase activity. Figure 3 shows that tropomyosin altered the inhibitory response of Cad35 in a manner similar to that typically observed with intact caldesmon. That is, the ATPase activity decreased in a linear manner with increasing Cad35 concentrations in the absence of tropomyosin. In the presence of tropomyosin the ATPase activity decreased more sharply at low Cad35 concentrations but less sharply at high Cad35 concentrations. The concentration of Cad35 required for 50% inhibition was 4.5 times greater in the absence of tropomyosin.

Cad35 inhibited both the ATPase activity and the fraction of S1 bound to actin during steady-state ATP hydrolysis (Figure 4). Higher actin concentrations were used here to increase the fraction of S1 bound to actin. The concentration of S1 used in binding experiments was reduced relative to that used in ATPase measurements to eliminate the possibility of ATP depletion during the binding assays. Both curves are compared to the calculated fraction of bare actin (1 − theta shown as broken lines) since this fraction decreases with increasing Cad35 concentrations. The fraction of bare actin was calculated from the binding parameters for Cad35 using the McGhee and von Hippel equation and an actin concentration of 50 μM. The decrease in the fraction of S1−ATP bound was great enough to account for most of the inhibition of ATPase activity; 50% inhibition of ATPase activity occurred at a total caldesmon concentration of 6 μM whereas 50% inhibition of binding required approximately 9 μM Cad35. The key point here is that caldesmon inhibits the binding of S1−ATP to actin even in the presence of tropomyosin.

The binding of Cad35 to actin and actin−tropomyosin was measured at several ionic strength conditions to facilitate the

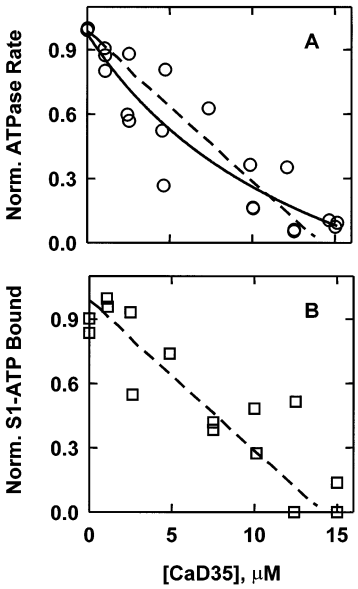

FIGURE 4: Effect of Cad35 on inhibition of ATPase activity and binding of S1 to actin−tropomyosin during ATP hydrolysis. Conditions: 50 μM actin, 11 μM tropomyosin, 0.1 μM S1 (binding) or 1 μM S1 (ATPase), 2 mM MgATP, 2 mM $MgCl_2$, 29 mM potassium propionate, 1 mM EGTA, 5 mM dithiothreitol, and 10 mM imidazole, pH 7, at 25 °C. (A) Normalized ATPase rate for two preparations of Cad35 shown together with a theoretical curve for the fraction of actin sites unoccupied by Cad35. (B) Normalized fraction of S1 bound during steady-state ATP hydrolysis shown with a theoretical curve for the fraction of actin sites unoccupied by Cad35.

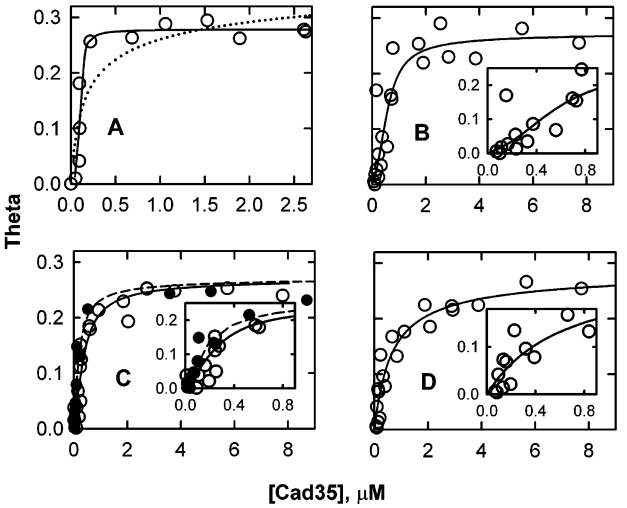

FIGURE 5: Binding of Cad35 to actin (open symbols) and actin−tropomyosin (closed symbols). Conditions: 5 μM actin ± 1.1 μM tropomyosin at 25 °C with buffers prepared as in Figure 1. All theoretical curves shown are for $n = 3.6$ (solid curves). (A) 60 mM ionic strength, $K = 0.11\ \mu M^{-1}$, and $\omega = 88$. The dotted line shows the best fit with the constraint so that $n = 2$. (B) 90 mM ionic strength, $K = 0.13\ \mu M^{-1}$, and $\omega = 12$. (C) 115 mM ionic strength, $K = 0.36\ \mu M^{-1}$, and $\omega = 5.7$ in the absence of tropomyosin (open symbols) and $K = 0.84\ \mu M^{-1}$ and $\omega = 4.6$ in the presence of tropomyosin (solid symbols). (D) 165 mM ionic strength, $K = 0.36\ \mu M^{-1}$, and $\omega = 3.4$.

detection of multiple populations of binding sites. Figure 5A shows the binding of Cad35 to pure actin at 50 mM ionic strength. The data are well described by a theoretical curve with $n = 3.6$. The data are not well described by curves for $n = 2$ (dotted line), and no combination of values of K and ω could produce a reasonable curve for $n = 1$. Increasing

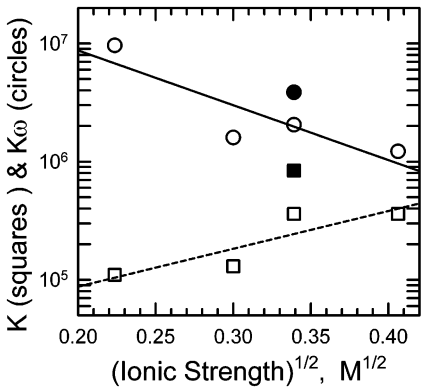

FIGURE 6: Effect of ionic strength on the parameters defining the binding of Cad35 to actin (open symbols) and actin−tropomyosin (closed symbols).

the ionic strength to 90 (Figure 5B), 115 (Figure 5C), and 165 mM (Figure 5D) lowered the affinity but did not appreciably change the number of actin monomers in a binding site. In no case was there an indication of multiple phases. This can be seen most clearly in the insets to curves B−D that show the initial part of the curves. Tropomyosin enhanced the binding of Cad35 to actin but did not otherwise change the binding isotherm (Figure 5C). In the presence of tropomyosin there was no evidence of multiple populations, and the value of n was the same as in the absence of tropomyosin.

Figure 6 shows the value of K and the product $K\omega$ as a function of the square root of the ionic strength. The product $K\omega$ is the affinity of caldesmon on a singly contiguous site. This value decreased with increasing ionic strength. The value of K, the affinity of caldesmon to an isolated site of 3.6 actin monomers, increased with increasing ionic strength while the interactions among contiguous Cad35 molecules, given by ω, were less favorable. As a result, the value of $K\omega$ decreased. Tropomyosin increased both the value of K and the product $K\omega$ to a similar degree as seen earlier with caldesmon.

DISCUSSION

Both caldesmon and troponin inhibit actin-activated ATP hydrolysis by myosin. The former is thought to be a modulator of smooth muscle contraction while troponin is known to be the key regulator of contraction in striated muscle. The inhibition of actin-activated ATPase activity by either caldesmon or troponin is enhanced by tropomyosin. Our earlier data suggested that the mechanisms of inhibition by caldesmon and troponin are focused at different steps of the ATPase cycle (*15*). Others believe that caldesmon functions much like troponin (*18*, *48*). These views are based on several differences in observations such as the manner in which caldesmon binds to actin.

If caldesmon behaved more like troponin, then it would stabilize tropomyosin into an inhibitory state. Like troponin, one caldesmon might bind to a single actin monomer but extend its influence through 7 actin monomers or some multiple of 7 actin monomers. Those who favor this model generally assume that 1 caldesmon molecule influences 14 actin monomers. Small caldesmon fragments are thought to bind to actin in much the same way as intact caldesmon binds (*18*, *19*). A description of this view and a model of caldesmon

binding to actin can be found elsewhere (*49*). However, we suggest that inhibition of S1−ATP binding has an important role in the inhibition of ATPase activity by caldesmon. The ability of caldesmon to inhibit myosin binding is dependent on the number of actin monomers that are in contact with caldesmon. Likewise, the number of actin monomers in contact with caldesmon changes with the size of caldesmon.

The present study supports the latter case. The binding of both intact caldesmon and recombinant Cad35 is fit well by the McGhee and von Hippel equation for a single class of binding sites. The binding of intact caldesmon to F-actin or F-actin−tropomyosin is consistent with an interaction with about 7 actin monomers. In some cases we found a better fit with $n = 5$. This could be due to some nonspecific binding at high caldesmon concentrations or binding of some caldesmon to caldesmon that is already bound to actin. The difference between fitted curves for $n = 5$ and $n = 7$ is small. Our working assumption is that the stoichiometry of caldesmon binding is the same as the stoichiometry of tropomyosin binding or $n = 7$.

We have not observed qualitative differences in the binding to actin compared to actin−tropomyosin in the present study nor in our earlier work despite our use of assays based on radioactivity (*10*), fluorescence changes (*41*), and in the present case unlabeled proteins or proteins labeled with the fluorescent probe IANBD, using either polyacrylamide gel electrophoresis or reverse-phase HPLC to measure the bound caldesmon. We have obtained consistent results with both heat-treated and non-heat-treated caldesmon and with caldesmon fragments that were prepared by digestion of intact caldesmon or expressed in bacteria. Changes in ionic strength do not result in qualitatively different data. In all cases the data are consistent with a single class of binding sites in which caldesmon interacts with several actin monomers. It is also interesting that simulations of binding with the assumption of two populations of sites did not predict a discontinuity in the binding isotherms (see Appendix). In the absence of strong evidence for multiple site binding we suggest that caldesmon binds to a single population of sites on actin with each site consisting of about 7 actin protomers.

Reasonable but not "best fits" to the binding data could be obtained by constraining ω to give negative cooperativity ($0 < \omega < 1$). Under this constraint it was possible to fit the binding data to $n = 3$. Values of $n = 1$ were impossible in some cases, and even $n = 2$ produced a poor fit. However, negative cooperativity with $n = 3$ is unlikely based on electron microscopic images of caldesmon showing clustering of caldesmon on actin filaments (*50*). This is suggestive of positive cooperativity. Electron microscopy also shows a spacing of caldesmon equivalent to that of tropomyosin or 7 actin monomers (*51*, *52*). We suggest that caldesmon binds to about 7 actin monomers with positive cooperativity (*10*).

Cad35 bound to 3 actin monomers rather than 5−7 for intact caldesmon. This is in agreement with other data showing that the number of actin monomers interacting directly with caldesmon decreases in the order caldesmon > Cad35 > Cad20 > Cad7.3 = Cad10 (*21*, *28*−*30*). This bacterially expressed fragment shows no sign of a high-affinity site with $n = 14$ and a low-affinity site with $n = 1$ as proposed by others for another similarly sized expressed caldesmon fragment (*19*). Furthermore, the value of n is the same in the absence and presence of tropomyosin. This is quite unlike the case for troponin that binds with $n = 1$ in the absence of tropomyosin but with $n = 7$ in the presence of tropomyosin.

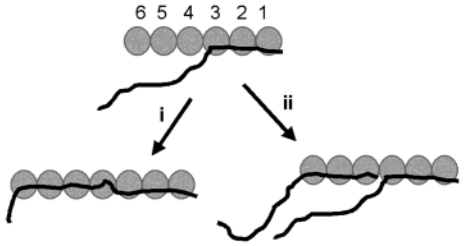

FIGURE 7: Possible mechanism of binding of whole caldesmon to a growing actin filament. The direction of chain growth is from 1 to 6. Pathway i shows binding that would occur if actin polymerization were very fast. Pathway ii shows that with slow actin polymerization attachment of a second caldesmon to a group of 3 actin monomers is faster than the addition of the seventh actin monomer that is required to stabilize the end of a single caldesmon molecule.

Rather than using caldesmon fragments, some laboratories have deleted selected regions from caldesmon to identify those sites that are important for various functions. Deletion of parts of the COOH-terminal region of caldesmon resulted in an increase in the apparent size of the actin binding site in some cases (*26*, *27*). This effect was seen in both the presence and absence of tropomyosin and cannot be attributed to long-range cooperativity through tropomyosin. In some cases it appeared as though a single caldesmon bound to 50−100 actin monomers (*26*). It is unlikely that these results imply a very long range through-actin effect of caldesmon. It is more likely that the true end point had not been reached in these studies because of a reduced affinity, the introduction of negative cooperativity (a consequence of the parking problem), or aggregation of the actin by the mutant molecules.

When high concentrations of caldesmon were added to G-actin together with divalent ions (to stimulate polymerization) and phalloidin (to stabilize actin in the filamentous state), it was possible to produce a complex where each caldesmon molecule was bound to approximately 3 actin monomers. Galazkiewicz et al. made a similar observation (*53*). Their study was designed to determine if caldesmon stimulates actin polymerization, so they did not add salt or phalloidin to stabilize the actin polymer. Nevertheless, the basic observations were similar. We interpret these observations as evidence for a two-step association of caldesmon with F-actin shown schematically in Figure 7. We suggest that caldesmon interacts most strongly with 3 actin monomers and that there is a weaker interaction with 4 additional actin monomers. That is, a single caldesmon molecule seems to interact in a heterogeneous fashion with each protomer in a unit of 7 actin monomers independent of the presence of tropomyosin (*54*). This is different from the view that there are two sites for caldesmon binding ($n = 1$ and $n \geq 14$) with the latter existing only in the presence of tropomyosin.

If a single caldesmon molecule binds tightly to 3 actin monomers and weakly to 4 actin monomers, as we have suggested, why is the interaction with 3 monomers favored with a growing actin filament? Consider a growing actin filament that has 1 caldesmon bound to 3 actin monomers as shown in top of Figure 7. As the fourth, fifth, and sixth monomers are added, the caldesmon has little tendency to

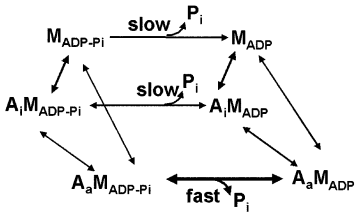

FIGURE 8: Hill et al. model of regulation. Actin−tropomyosin is distributed between an inactive state, A_i, and an active state, A_a. Myosin has many possible chemical states, but only two are shown: post ATP cleavage, M_{ADP-P_i}, and post phosphate release, M_{ADP}. Inhibition of ATP hydrolysis can occur as a result of inhibition of myosin binding to actin or to stabilization of state A_i or by directly reducing the rate constant for a transition between two A_aM states.

bind to these residues. Once the seventh monomer is added, there is sufficient additional binding energy to hold the caldesmon down along the entire stretch of 7 actin monomers as in pathway i. But actin binding to caldesmon is a rapid process (*41*) compared to actin filament elongation. This means that a second caldesmon molecule can bind to actin residues 4−6 before actin monomer 7 is added to the chain as in pathway ii. Thus, the case described is kinetically limited to $n = 3$.

Our bacterially expressed Cad 35 inhibited both the binding of S1−ATP to actin−tropomyosin as well as the actin-activated ATPase rate (Figure 4). As we have seen before with intact caldesmon (*8*, *14*) and the 20 kDa fragment (*55*), the ATPase rate decreased to a slightly greater extent than the binding of S1−ATP to actin. Another group observed little decrease in S1−ATP binding until the caldesmon (*18*) or caldesmon fragment concentration was very high (*19*). We have explored this question in an earlier report and have found that inhibition of S1−ATP binding can be obscured under certain conditions (*14*). In addition to these observations in solution, we have also found that intact caldesmon and several caldesmon fragments from the COOH-terminal region of caldesmon inhibit myosin cross-bridge binding in skeletal muscle fiber preparations (*47*).

Low concentrations of Cad35 inhibit the actin-activated ATPase activity of S1 to a greater extent in the presence of tropomyosin (Figure 3). Similar results were obtained with intact caldesmon (*9*, *10*) and with fragments produced by enzymatic digestion of intact caldesmon. We suggested earlier that this behavior might be due to a dual role of caldesmon. Caldesmon inhibits the binding of S1 to actin in both the presence and absence of smooth muscle tropomyosin. Caldesmon may also reverse the normal activating effect that smooth muscle tropomyosin has on ATPase activity (*56*, *57*).

The ultimate goal of examining caldesmon binding to actin is to understand the mechanism of inhibition of ATPase activity. It is instructive to compare the regulatory activity of caldesmon to that of troponin. The model of Hill et al. shown in Figure 8 (*58*) illustrates several possible loci of regulation. This model accurately simulates the steady-state effect of troponin−tropomyosin on ATPase activity (*58*) and is consistent with the effect of troponin−tropomyosin on the equilibrium binding of S1−nucleotide complexes to actin (*59*) as well as the kinetics of S1 binding (*60*). In this model, S1 can hydrolyze ATP along three pathways. Hydrolysis is slow when the S1 is detached from actin. Actin-activated ATPase activity is high only when S1 is bound to actin in the active state, A_a. Possible points of regulation are the binding of one or more myosin−nucleotide states to actin, the transition of actin−myosin from an A_i state to an A_a state, and direct modulation of transitions along the pathway of state 2. An example of the last case would be a reduction in the rate of P_i release from the $A_aM_{ATP-P_i}$ state. We propose that troponin−tropomyosin controls the transition of actin from the inactive state A_i to the active state A_a with little effect on binding of myosin to actin during ATP hydrolysis (*61*). Caldesmon has a greater role in inhibiting the binding of myosin to actin (Figure 8) although it is likely that other factors also play a role (in our minds a lesser role).

Tropomyosin appears to play a different role in regulation of caldesmon compared with troponin. As shown here, tropomyosin strengthens the binding of caldesmon but does not change the stoichiometry of binding as it does with troponin. Tropomyosin is essential for the inhibition of the rate of S1 binding to actin by troponin but not by caldesmon (*15*). Troponin inhibits the equilibrium binding of S1 to actin but only in the absence of tropomyosin. In contrast, caldesmon inhibits the equilibrium binding of S1 to actin in the presence and absence of tropomyosin (*61*). This inhibition of S1 binding is enhanced to a small degree by the presence of tropomyosin (*15*). We have also observed that caldesmon reduces the rate of release of mant-ATP from S1−actin regardless of the presence of tropomyosin (*62*). Two laboratories have reported that caldesmon induces cooperative binding of S1 to actin as observed with tropomyosin−troponin (*48*, *63*, *64*). However, in the case of caldesmon this may not be real cooperativity. Rather, increasing concentrations of S1 tend to displace caldesmon from actin, causing an apparent increase in the S1 affinity with increasing S1 concentrations (*15*). A model in which caldesmon and S1 competitively interact with actin yields the same predicted binding curves as might be expected from true cooperativity. Thus there is no clear evidence that caldesmon shifts the equilibrium between states 1 and 2 of actin to a large extent as in the case of troponin.

Caldesmon may affect steps other than the binding of S1 to actin, but there is disagreement over the relative importance of such events. We observed that caldesmon had a large effect on the K_M for actin-activated ATPase activity and a small effect on the k_{cat} (*65*), supporting a minor role of regulation of a kinetic transition. Another laboratory reported a larger effect of caldesmon on the k_{cat} than we observed, but like us they observed a substantial inhibition of binding and a change in the K_M (*66*). However, another laboratory reported that the full inhibitory effect was due to a reduction in the k_{cat} (*67*). That latter study is inconsistent with our results. Our indications from studies with mant-ATP release are that a step in addition to S1 binding to actin may be altered somewhat by caldesmon (*62*). If caldesmon does alter the equilibrium of actin−tropomyosin to favor an inactive state, this change must be novel. Reconstructions of electron micrographs of actin−caldesmon−tropomyosin show that caldesmon moves tropomyosin in the *opposite* direction than troponin does in striated muscle (*11*).

Caldesmon binding data from different laboratories are similar (*2*, *68*) but differ by small deviations at low caldesmon concentrations in the presence of tropomyosin (*9*, *19*). We have failed to find experimental support for a

transition that could be interpreted as two types of caldesmon binding in the presence of tropomyosin. Is it possible that these transitions are real and that we and other laboratories have failed to observe them? One approach to this problem is to rigorously analyze available data in terms of a model for two-site binding.

Reports describing two populations of binding relied on Scatchard plots to analyze caldesmon binding data (*9*, *19*). The Scatchard analysis was derived for binding of a ligand to a single site of a macromolecule with multiple sites (*69*). However, this is not the case with caldesmon. Rather, the ligand caldesmon interacts with several actin monomers in an actin filament. Binding of a long ligand to a lattice involves a parking problem and the potential for cooperativity as already described. These factors cause Scatchard plots to be nonlinear even in cases of a homogeneous class of binding sites (*44*). Thus a Scatchard analysis may be misleading. The appropriate model for simulating binding of a ligand to a binding site consisting of multiple protomers is that developed by McGhee and von Hippel (*44*). Their formalism is general and may be extended to the case where there are two or more different types of binding sites. The analysis of several experimental binding curves with multiple class binding site models is shown in the appendix. The models analyzed could not duplicate observed transitions in caldesmon binding curves. We conclude that caldesmon binds to actin and actin−tropomyosin uniformly, in which a binding site is composed of about 7 actin monomers. Furthermore, binding occurs with slight positive cooperativity and may involve an intermediate state where the COOH terminus of caldesmon is bound to 3 actin monomers.

ACKNOWLEDGMENT

The authors thank Mr. Michael Vy-Freedman for excellent technical assistance and Dr. Mechthild Schroeter for critical reading of the manuscript.

APPENDIX[2]

Simulation of Caldesmon Binding to Actin and Actin−Tropomyosin with Two-State Models

Figure 9 shows contrasts of two models of caldesmon binding. In model I caldesmon binds to 7 actin protomers, but binding occurs with an intermediate state with caldesmon attached to 3 protomers. The alternative, model II, has two stable binding states. State 1 binds to actin tightly with $n > 14$, and state 2 binds to actin less tightly with $n = 1$. These states might be static or they may be in a rapid equilibrium with each other. Does a two-state model simulate the data more accurately than the single state model used in the analyses thus far?

The Two-State Model. The McGhee and von Hippel model can be revised to describe the binding of each ligand species as a function of its free ligand concentration and of the binding of all the other ligand species. This situation is formally equivalent to a homogeneous ligand binding in different and noninterfering ways to a single lattice. The only difference between these cases is that in the first case the total number of binding sites is the same for all ligands and

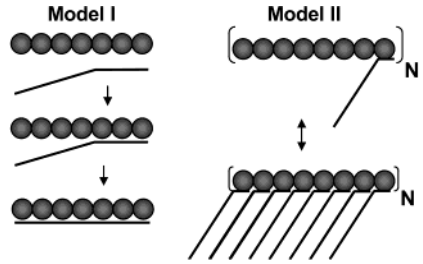

FIGURE 9: Possible models of actin binding to caldesmon. Model I shows binding to a single site of 7 actin protomers. In the intermediate state each caldesmon interacts tightly with 3 actin protomers. Binding could occur with negative, positive, or no cooperativity. Model II is a two-state model. In the absence of tropomyosin, binding can only occur to the lower affinity state 2 in which each caldesmon binds to a single actin protomer. In the presence of tropomyosin, binding can also occur to the higher affinity state 1 where each binding site consists of 14 or more protomers. If there is no interconversion between states 1 and 2 the caldesmon will first populate the high-affinity state with the larger value of n and then occupy the low-affinity sites. In the case of a rapid equilibrium between the two states, the occupancy of state 1 decreases as the occupancy of state 2 increases.

in the second case the total ligand concentration is the same. Therefore, while we are considering the hypothesis that there are different kinds of binding sites on actin for caldesmon, the simulations could also be interpreted in terms of multiple kinds of ligands.

Equation 1 can be extended to a multiple state case where several populations of binding sites are available for ligand binding. Consider the case of ligand binding to two different populations of binding sites on lattice. The left part of the equation represents the unknowns ν and L, and the right side is a function dependent on all numbers of populations of binding sites. The equation can be written as

$$\frac{\nu_i}{L_i} = K_i\left(1 - \sum_i n_i\nu_i\right) \times \left(\frac{(2\omega_i - 1)\left(1 - \sum_i n_i\nu_i\right) + \sum_i \nu_i - R_i}{2(\omega_i - 1)\left(1 - \sum_i n_i\nu_i\right)}\right)^{n_i - 1} \times \left(\frac{1 - \sum_i (n_i\nu_i + \nu_i) + R_i}{2\left(1 - \sum_i n_i\nu_i\right)}\right)^2 \quad (2)$$

where

$$R_i = \sqrt{\left(1 - \sum_i (n_i + 1)\nu_i\right)^2 + 4\omega_i \sum_i \nu_i (1 - n_i\nu_i)}$$

Index i shows that a parameter is associated with the ith binding site, and ν_i is the ratio of caldesmon bound to the ith population ligand to the total lattice concentration. Because there is only a single species of ligand, L_i is the same for all equations in the set (eq 2), i.e., $L_i = L$. The summation signs in the right part of the equation include binding of ligands to every binding site. This equation might be generalized to the simple form:

[2] This appendix was contributed by B. Gafurov and J. M. Chalovich.

$$\frac{\nu_i}{L} = F_i(\nu_{1...N})$$

We are most interested in the simple case of two different populations of lattice, so the set of two equations has to be drawn:

$$F_1(\nu_1,\nu_2) - \frac{\nu_1}{L} \equiv f_1(\nu_1,\nu_2) = 0$$

$$F_2(\nu_1,\nu_2) - \frac{\nu_2}{L} \equiv f_2(\nu_1,\nu_2) = 0 \qquad (3)$$

The variables cannot be separated in these complex functions. Newton's method was used to solve this set of equations, where functions f_1 and f_2 were put in a Taylor's series and linearized (*70*). The following set of equations was obtained for the Taylor's series at the 0 point:

$$f_1(\nu_1,\nu_2) \cong f_1(\nu_1,\nu_2)_{\nu_1,\nu_2=0} + \nu_1 f_1(\nu_1,\nu_2)'_{\nu_1}|_{\nu_1,\nu_2=0} + \nu_2 f_1(\nu_1,\nu_2)'_{\nu_2}|_{\nu_1,\nu_2=0}$$

$$f_2(\nu_1,\nu_2) \cong f_2(\nu_1,\nu_2)_{\nu_1,\nu_2=0} + \nu_1 f_2(\nu_1,\nu_2)'_{\nu_1}|_{\nu_1,\nu_2=0} + \nu_2 f_2(\nu_1,\nu_2)'_{\nu_2}|_{\nu_1,\nu_2=0}$$

or in simplified form:

$$a_1 + b_1\nu_1 + c_1\nu_2 = 0$$

$$a_2 + b_2\nu_1 + c_2\nu_2 = 0$$

where a_i are functions and b_i and c_i are their partial derivatives calculated at the zero point; i.e., they are constants.

This set of linear equations can be solved, and functions ν_i can be derived:

$$\nu_1 = \frac{a_1c_2 - a_2c_1}{b_2c_1 - b_1c_2} \qquad \nu_2 = \frac{a_2b_1 - a_1b_2}{b_2c_1 - b_1c_2}$$

Partial derivatives b_i and c_i were calculated numerically during the simulations. The initial conditions for ν_i were assumed to be zero at minimal appropriate L ($L \rightarrow 0$).

Finally, the sum of ν_i was fitted to the experimental binding measurements using the least sum of square differences taken between the simulated resultant $\nu_1 + \nu_2$ curve and experimental points. The values of n_i, ω_i, and K_i were allowed to float to obtain the best fit as defined by the minimalization of the sum of squares.

The precision of the parameters predicted by the two-state model was sensitive to the numerical method used to solve the set of nonlinear equations (eq 3). There is no way to directly solve that kind of set of equations. The values of n, ω, and K are approximate. The method used gives only linear (rough) estimations of the functions, so that error in calculations might be of the first order. Errors in parameters were estimated on the basis of the standard deviation of the simulated curve to be less than 10%. To test the model, we simulated the binding with one of the populations set to zero. As predicted, that special case gave the same result as the regular McGhee and von Hippel equation.

Fitting a model for two classes of binding sites to a single data curve does not give a unique solution. To ensure that the results were reasonable, we fixed the properties of one of the types of binding sites and let the parameters for the others float. The parameters used to fix one population were chosen to conform to the various published reports on caldesmon binding. We also restricted the fitting so that 1 > theta > 0 and that the first derivative of each binding curve is ≥0 in the noninterconversion case. Simulations were made on a personal computer using the Delphi3.0 programming language.

Intact Caldesmon Binding to F-Actin. Figure 10 shows the fitting of two-site models to the binding of intact caldesmon to actin and actin−tropomyosin. Panels A and B of Figure 10 contain data from Figure 1. These data do not exhibit biphasic binding. The curves shown are for a two-site binding model where there was no change in the distribution of the two sites as the caldesmon concentration was increased. In the presence of tropomyosin the best fit was with $n_1 = 6.7$, $\omega_1 = 3.4$, $K_1 = 2.6$ and $n_2 = 6.7$, $\omega_2 = 3.4$, $K_2 = 0.21$ (dashed and dotted lines of Figure 10A) for the first and second population of binding sites (or primary and secondary), respectively. The parameters for both sites are nearly the same so there appears to be only a single site in this case. In the absence of tropomyosin (Figure 10B) the parameters for the two-site model were $n_1 = 4.1$, $\omega_1 = 2.6$, $K_1 = 2.6$ and $n_2 = 7.9$, $\omega_2 = 4.4$, $K_2 = 0.71$ (dashed and dotted lines, respectively). In both the presence and absence of tropomyosin the curves generated by one- and two-site models were virtually identical, having correlation coefficients between the simulated curve and experimental points of about 0.95−0.99. Furthermore, the distribution between states 1 and 2 (Figure 9, model II) was not greatly changed by the addition of tropomyosin. The pattern does not support the hypothesis that there are two populations of binding in the presence of tropomyosin but only one in the absence of tropomyosin. Similar results were obtained for fitting the two-site model to our data from higher ionic strength conditions (not shown).

Panels C and D of Figure 10 show the fit of both the one-state model and the two-state model to the data of Smith et al. (*9*). These data were converted from the Scatchard plot in that paper. They interpreted the data with tropomyosin (Figure 10C) as binding to high-affinity sites composed of >14 actin protomers and to low-affinity sites in a 1:1 complex. The original analysis of the 685C data by Scatchard plots yielded the following values: $B_{max} = 0.027 \pm 0.032$ and 0.39 ± 0.03 and $K_d = 0.11 \pm 0.46$ and 14.9 ± 4.7 μM for the first population and second population, respectively (*19*). The uncertainty in the parameters for the first population suggests that this population may not be significant.

Our analysis with a single site model (solid line) gave $n = 1.9$, $\omega = 2.9$, and $K = 0.16$. The value of n near 2 results from the high point at the highest free caldesmon concentration. Elimination of that high point from the fit gave parameters that were similar to those obtained from an analysis of the data from other laboratories (*2*). More data at higher caldesmon concentrations would be required to define the end point. The data could also be fit with the constraint of the negative cooperativity model ($0 < \omega < 1$) with the parameters $n = 1.1$, $\omega = 0.55$, and $K = 0.28$ (fit not shown). The fit with negative cooperativity was slightly worse than for that with slight positive cooperativity. The data of Figure 10C were also analyzed with a two-site model

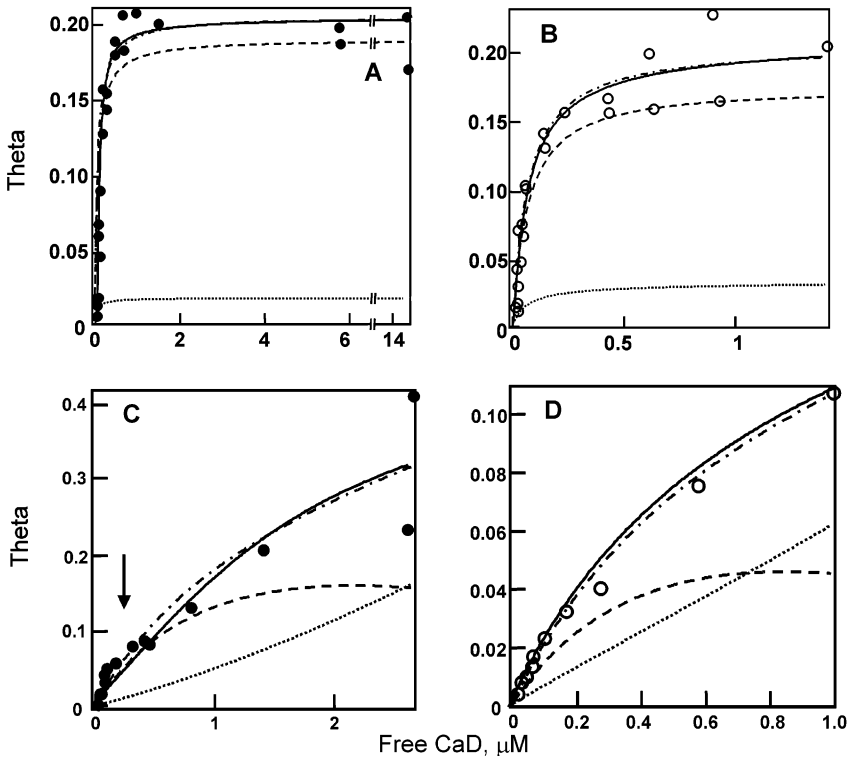

FIGURE 10: Analysis of binding of whole caldesmon to actin in the absence (open symbols) and presence (closed symbols) of tropomyosin. Theta (the ratio of caldesmon bound to actin total) is plotted against the free caldesmon concentration. Solid lines are best fits of the one-site McGhee and von Hippel model I to the experimental points. The alternating dash−dot line is the theoretical total binding for the two-site McGhee and von Hippel model II without rapid equilibrium between the states (see Figure 9); the dashed and dotted lines are binding to states 1 and 2, respectively. (A) and (B) are from Figure 1A while (C) and (D) are from ref *9*.

with no interconversion between sites (dash−dot line). This model was not able to simulate the observed break in the data, and we conclude that a two-state model is not a better representation of the data than the one-state model. The parameters of the fit were $n_1 = 3.4$, $\omega_1 = 2.0$, and $K_1 = 0.2$ (dashed line) and $n_2 = 1.8$, $\omega_2 = 1.2$, and $K_2 = 0.04$ (dotted line). State 1 accounted for 63% of the total binding.

There was no break in the binding curve in the absence of tropomyosin (Figure 10D), but the free caldesmon concentration may not have been high enough to see the break (compare to Figure 10C). The best fit of the data of Figure 10D without any constraints on the cooperativity is shown with a solid line. The fitted parameters were $n = 3.4$, $\omega = 1.01$, and $K = 0.26$ (solid curve). The value of n is unreliable because the binding curve did not reach a plateau. The binding curve in Figure 10D could also be interpreted with the constraint of negative cooperativity. Fitting the data with the constraint of negative cooperativity produced the values $n = 2.9$, $\omega = 0.6$, and $K = 0.26$ (curve not shown). The parameters for a two-site fit for binding to pure actin (Figure 10D dash−dot line) were $n_1 = 3.8$, $\omega_1 = 3.6$, $K_1 = 0.18$ and $n_2 = 1.6$, $\omega_2 = 1.21$, $K_2 = 0.07$, with state 1 constituting 53% of total binding. That is, in the two-state model the addition of tropomyosin changes the fraction of caldesmon bound to state 1 from 53% to 63%; this is not significant. It is also noteworthy that the best fit of the model does not predict either state 1 to be greater than 14 protomers or state 1 to be 1 protomer.

Low Molecular Mass Mutant Caldesmon Binding to F-Actin. Redwood and Marston have observed an even more pronounced biphasic binding curve with a fragment from the COOH-terminal region of caldesmon, caldesmon 685C (*19*). This fragment is only about 25% as large as intact caldesmon. Their data for binding to actin−tropomyosin and pure actin are shown in panels A and B of Figure 11, respectively. The arrow in Figure 11A shows the step in the data that was interpreted as a transition from high-affinity binding to a site with $n = 14-20$ to low-affinity binding to a site with $n = 1-2$. Panels A and B of Figure 11 also show the predictions of the regular one-site binding McGhee and von Hippel model (solid lines). In the presence of tropomyosin the parameters were $n = 1.4$, $\omega = 1.3$, and $K = 0.06$. In the absence of tropomyosin the parameters were $n = 1.8$, $\omega = 2.8$, and $K = 0.03$. The values of n for this small fragment are similar to those obtained with another similarly sized caldesmon fragment produced by digestion with chymotrypsin (*29*). Note that the values of cooperativity obtained for the data of Figure 11 were small; short caldesmon mutants may lack the sequences essential for tandem caldesmon−caldesmon interactions. The single state model gave a reasonable fit to the data in both the presence and absence of tropomyosin, but it did not precisely follow the points in the region of the transition shown by the arrow in Figure 11A.

Two types of two-state model were applied to these data in an attempt to duplicate the transition observed in Figure 11A. Results of the two-state model with no interconversion between sites are shown on Figure 11A,B by dash−dot lines with the following parameters: $n_1 = 1.64$, $\omega_1 = 1.29$, $K_1 = 0.034$; $n_2 = 3.6$, $\omega_2 = 2.14$, $K_2 = 0.011$ (with tropomyosin) and $n_1 = 1.44$, $\omega_1 = 1.22$, $K_1 = 0.033$; $n_2 = 1.44$, $\omega_2 = 1.22$, $K_2 = 0.022$ (without tropomyosin). The fraction of actin in state 1 with tropomyosin was about 60%; when tropomyosin was absent, it was about 45%. In the absence of

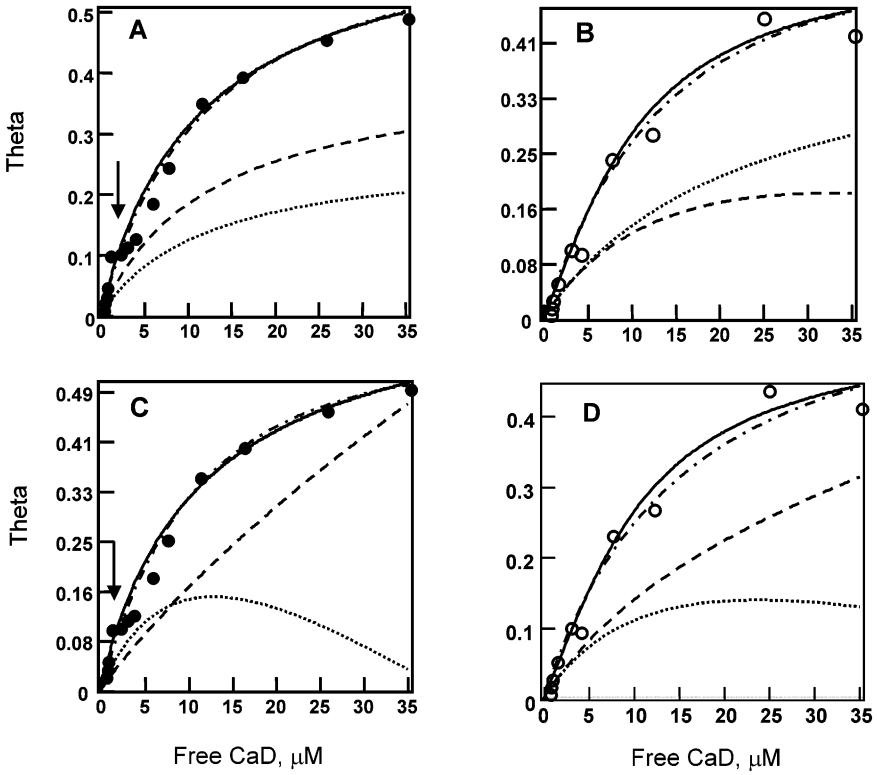

FIGURE 11: Analysis of the 685C caldesmon fragment binding to actin in the presence (A, C) and absence (B, D) of tropomyosin. Data are from ref *19*. Solid lines are best fits of the one-site McGhee and von Hippel model I to the experimental points. The alternating dash−dot line is the theoretical total binding for the two-site McGhee and von Hippel model II; the dashed and dotted lines are binding to states 1 and 2, respectively. (C) and (D) show the best fit of model II to the same data when states 1 and 2 are interconvertible while in (A) and (B) they are not (see Figure 9).

tropomyosin the properties of the two states were almost identical, indicating that the data are well described by a single state model.

These data were also examined by using a two-state model with a rapid equilibrium between states. Panels C and D of Figure 11 show that the value of theta for state 1 decreased, permitting more binding to state 2 as the concentration of caldesmon increased. The parameters for the first and second binding were $n_1 = 1.9$, $\omega_1 = 1.4$, $K_1 = 0.04$; $n_2 = 1.8$, $\omega_2 = 1.4$, $K_2 = 0.02$ with tropomyosin 83% in state 1 and $n_1 = 1.9$, $\omega_1 = 1.4$, $K_1 = 0.02$; $n_2 = 1.6$, $\omega_2 = 1.3$, $K_2 = 0.02$ without tropomyosin within 63% in state 1. While tropomyosin caused a change in the distribution, there was no significant difference between states 1 and 2 in either the presence or absence of tropomyosin. That is, there was no clear indication of multiple types of states. Neither two-state model could reproduce the step in binding data observed in the presence of tropomyosin.

Intact Caldesmon Binding to G-Actin. Figure 2 showed that the binding of caldesmon to growing actin filaments saturated at 1 caldesmon per 3 actin protomers. Could the value of *n* really be as small as 1 if evaluated by a two-state model? Simulation of the two-state model without interconversion gave a best fit with $n_1 = 3.5$, $\omega_1 = 2.1$, $K_1 = 0.3$ and $n_2 = 3.5$, $\omega_2 = 2.1$, $K_2 = 0.1$ with 75% of the binding to state 1. An analysis with a two-state model with rapid equilibrium between states is shown giving a best fit with $n_1 = 3.6$, $\omega_1 = 2.2$, $K_1 = 0.4$ and $n_2 = 3.0$, $\omega_2 = 1.9$, $K_2 = 0.06$ (60% and 40% first and second fractions). Neither model predicted a population of sites with $n = 1$ (not shown).

REFERENCES

1. Sobue, K., Muramoto, Y., Fujita, M., and Kakiuchi, S. (1981) *Proc. Natl. Acad. Sci. U.S.A. 78*, 5652−5655.
2. Chalovich, J. M., and Pfitzer, G. (1997) in *Cellular aspects of smooth muscle function* (Kao, C. Y., and Carsten, M. E., Eds.) pp 253−287, Cambridge University Press, Cambridge.
3. Dabrowska, R., Goch, A., Galazkiewicz, B., and Osinska, H. (1985) *Biochim. Biophys. Acta 842*, 70−75.
4. Smith, C. W. J., and Marston, S. B. (1985) *FEBS Lett. 184*, 115−119.
5. Sobue, K., Takahashi, K., and Wakabayashi, I. (1985) *Biochem. Biophys. Res. Commun. 132*, 645−651.
6. Ngai, P. K., and Walsh, M. P. (1985) *Biochem. J. 230*, 695−707.
7. Lash, J. A., Sellers, J. R., and Hathaway, D. R. (1986) *J. Biol. Chem. 261*, 16155−16160.
8. Chalovich, J. M., Cornelius, P., and Benson, C. E. (1987) *J. Biol. Chem. 262*, 5711−5716.
9. Smith, C. W. J., Pritchard, K., and Marston, S. B. (1987) *J. Biol. Chem. 262*, 116−122.
10. Velaz, L., Hemric, M. E., Benson, C. E., and Chalovich, J. M. (1989) *J. Biol. Chem. 264*, 9602−9610.
11. Hodgkinson, J. L., Marston, S. B., Craig, R., Vibert, P., and Lehman, W. (1997) *Biophys. J. 72*, 2398−2404.
12. Hemric, M. E., and Chalovich, J. M. (1988) *J. Biol. Chem. 263*, 1878−1885.
13. Chen, Y., and Chalovich, J. M. (1992) *Biophys. J. 63*, 1063−1070.
14. Sen, A., and Chalovich, J. M. (1998) *Biochemistry 37*, 7526−7531.
15. Sen, A., Chen, Y. D., Yan, B., and Chalovich, J. M. (2001) *Biochemistry 40*, 5757−5764.
16. Horiuchi, K. Y., and Chacko, S. (1991) *Biochem. Biophys. Res. Commun. 176*, 1487−1493.
17. Chalovich, J. M. (1992) *Pharmacol. Ther. 55*, 95−148.
18. Marston, S. B., and Redwood, C. S. (1993) *J. Biol. Chem. 268*, 12317−12320.
19. Redwood, C. S., and Marston, S. B. (1993) *J. Biol. Chem. 268*, 10969−10976.

20. Bartegi, A., Fattoum, A., Derancourt, J., and Kassab, R. (1990) *J. Biol. Chem. 265*, 15231−15238.
21. Huber, P. A. J., Gao, Y., Fraser, I. D. C., Copeland, O., El-Mezgueldi, M., Slatter, D. A., Keane, N. E., Marston, S. B., and Levine, B. A. (1998) *Biochemistry 37*, 2314−2326.
22. Ngai, P. K., and Walsh, M. P. (1987) *Biochem. J. 244*, 417−425.
23. Horiuchi, K. Y., Miyata, H., and Chacko, S. (1986) *Biochem. Biophys. Res. Commun. 136*, 962−968.
24. Clark, T., Ngai, P. K., Sutherland, C., Groschel-Stewart, U., and Walsh, M. P. (1986) *J. Biol. Chem. 261*, 8028−8035.
25. Mahmood, R., Cremo, C., Nakamaye, K. L., and Yount, R. G. (1987) *J. Biol. Chem. 262*, 14479.
26. Wang, Z., Horiuchi, K. Y., and Chacko, S. (1996) *J. Biol. Chem. 271*, 2234−2242.
27. Wang, Z., and Chacko, S. (1996) *J. Biol. Chem. 271*, 25707−25714.
28. Yazawa, M., Yagi, K., and Sobue, K. (1987) *J. Biochem. (Tokyo) 102*, 1065.
29. Velaz, L., Chen, Y., and Chalovich, J. M. (1993) *Biophys. J. 65*, 892−898.
30. Chalovich, J. M., Bryan, J., Benson, C. E., and Velaz, L. (1992) *J. Biol. Chem. 267*, 16644−16650.
31. Lehman, W., Vibert, P., and Craig, R. (1997) *J. Mol. Biol. 274*, 310−317.
32. Schenk, P. M., Baumann, S., Mattes, R., and Steinbiss, H. H. (1995) *BioTechniques 19*, 196−200.
33. Seetharam, R., Heeren, R. A., Wong, E. Y., Braford, S. R., Klein, B. K., Aykent, S., Kotts, C. E., Mathis, K. J., Bishop, B. F., Jennings, M. J., and (1988) *Biochem. Biophys Res. Commun. 155*, 518−523.
34. Pedigo, S., and Shea, M. A. (1995) *Biochemistry 34*, 1179−1196.
35. Spudich, J. A., and Watt, S. (1971) *J. Biol. Chem. 246*, 4866−4871.
36. Eisenberg, E., and Kielley, W. W. (1972) *Cold Spring Harbor Symp. Quant. Biol. 37*, 145−152.
37. Kielley, W. W., and Harrington, W. F. (1960) *Biochim. Biophys. Acta 41*, 401−421.
38. Weeds, A. G., and Taylor, R. S. (1975) *Nature 257*, 54−56.
39. Bretscher, A. (1984) *J. Biol. Chem. 259*, 12873−12880.
40. Graceffa, P. (1992) *Biochim. Biophys. Acta 1120*, 205−207.
41. Chalovich, J. M., Chen, Y., Dudek, R., and Luo, H. (1995) *J. Biol. Chem. 270*, 9911−9916.
42. Gill, S. C., and von Hippel, P. H. (1989) *Anal. Biochem. 182*, 319−326.
43. Lowry, O. H., Rosebrough, N. J., Farr, A. L., and Randall, R. J. (1951) *J. Biol. Chem. 193*, 265−275.
44. McGhee, J. D., and von Hippel, P. H. (1974) *J. Mol. Biol. 86*, 469−489.
45. Chalovich, J. M., and Eisenberg, E. (1982) *J. Biol. Chem. 257*, 2432−2437.
46. Wang, Z., Yang, Z. Q., and Chacko, S. (1997) *J. Biol. Chem. 272*, 16896−16903.
47. Heubach, J. F., Hartwell, R., Ledwon, M., Kraft, T., Brenner, B., and Chalovich, J. M. (1997) *Biophys. J. 72*, A1348.
48. Marston, S. B., Fraser, I. D. C., and Huber, P. A. J. (1994) *J. Biol. Chem. 269*, 32104−32109.
49. Marston, S. B., and Huber, P. A. J. (1996) in *Biochemistry of smooth muscle contraction* (Barany, M., Ed.) pp 77−90, Academic Press, San Diego.
50. Mabuchi, K., Li, Y., Carlos, A., Wang, C. L., and Graceffa, P. (2001) *J. Muscle Res. Cell Motil. 22*, 77−90.
51. Lehman, W., Craig, R., Lui, J., and Moody, C. (1989) *J. Muscle Res. Cell Motil. 10*, 101−112.
52. Frisbie, S. M., Reedy, M. C., Yu, L. C., Brenner, B., Chalovich, J. M., and Kraft, T. (1999) *J. Muscle Res. Cell Motil. 20*, 291−303.
53. Galazkiewicz, B., Belagyi, J., and Dabrowska, R. (1989) *Eur. J. Biochem. 181*, 607−614.
54. Chen, Y. D., and Chalovich, J. M. (1992) *Biophys. J. 63*, 1063−1070.
55. Velaz, L., Ingraham, R. H., and Chalovich, J. M. (1990) *J. Biol. Chem. 265*, 2929−2934.
56. Williams, D. L., Greene, L. E., and Eisenberg, E. (1984) *Biochemistry 23*, 4150−4155.
57. Lehrer, S. S., and Morris, E. P. (1984) *J. Biol. Chem. 259*, 2070−2072.
58. Hill, T. L., Eisenberg, E., and Chalovich, J. M. (1981) *Biophys. J. 35*, 99−112.
59. Hill, T. L., Eisenberg, E., and Greene, L. E. (1980) *Proc. Natl. Acad. Sci. U.S.A. 77*, 3186−3190.
60. Chen, Y., Yan, B., Chalovich, J. M., and Brenner, B. (2001) *Biophys. J. 80*, 2338−2349.
61. Resetar, A. M., Stephens, J. M., and Chalovich, J. M. (2002) *Biophys. J. 83*, 1039−1049.
62. Resetar, A. M., and Chalovich, J. M. (1999) *Biophys. J. 76*, A282.
63. Ansari, S., El-Mezgueldi, M., and Marston, S. B. (2002) *Biophys. J. 82*, 375A.
64. Horiuchi, K. Y., and Chacko, S. (1989) *Biochemistry 28*, 9111−9116.
65. Hemric, M. E., Freedman, M. V., and Chalovich, J. M. (1993) *Arch. Biochem. Biophys. 306*, 39−43.
66. Horiuchi, K. Y., Samuel, M., and Chacko, S. (1991) *Biochemistry 30*, 712−717.
67. Marston, S. (1988) *FEBS Lett. 238*, 147−150.
68. Chalovich, J. M., Sen, A., Resetar, A., Leinweber, B., Fredricksen, R. S., Lu, F., and Chen, Y. D. (1998) *Acta Physiol. Scand. 164*, 427−435.
69. Scatchard, G. (1949) *Ann. N.Y. Acad. Sci. 51*, 660−672.
70. Householder, A. S. (1970) *The Numerical Treatment of a Single Nonlinear Equation*, McGraw-Hill, New York.

BI0274017